

Electromagnetic Implosion of Spherical Liner

J. H. Degnan, F. M. Lehr, J. D. Beason,* G. P. Baca, D. E. Bell, A. L. Chesley, S. K. Coffey,[†] D. Dietz, D. B. Dunlap,[‡] S. E. Englert, T. J. Englert, D. G. Gale,[‡] J. D. Graham,[‡] J. J. Havranek, C. D. Holmberg, T. W. Hussey, R. A. Lewis,[§] C. A. Outten, R. E. Peterkin, Jr., D. W. Price, N. F. Roderick, E. L. Ruden, U. Shumlak, G. A. Smith,[§] and P. J. Turchi

High Energy Plasma Division, Phillips Laboratory, Kirtland Air Force Base, New Mexico 87117-5776

(Received 12 April 1994)

We have magnetically driven a tapered-thickness spherical aluminum shell implosion with a 12.5 MA axial discharge. The initially 4 cm radius, 0.1 to 0.2 cm thick, $\pm 45^\circ$ latitude shell was imploded along conical electrodes. The implosion time was approximately 15 μsec . Radiography indicated substantial agreement with 2D-MHD calculations. Such calculations for this experiment predict final inner-surface implosion velocity of 2.5 to 3 cm/ μsec , peak pressure of 56 Mbar, and peak density of 16.8 g/cm³ (>6 times solid density). The principal experimental result is a demonstration of the feasibility of electromagnetic-driven spherical liner implosions in the cm/ μsec regime.

PACS numbers: 52.55.Ez, 52.50.Lp

A crucial problem in the creation of high energy density matter is spherically symmetric implosions. Laser techniques become quite expensive at high total energy in the compressed matter. Electromagnetic implosions, on the other hand, require close control of solid state mechanics at high magnetic field values.

Fast solid density shell implosions, particularly in spherical geometry, may be used to obtain physical regimes of 10 to 100 Mbar pressures with 1 to 10 g masses in the laboratory. Such regimes can be useful for studies of equation of state of materials and for applications including magnetized target fusion [1]. We have previously worked on electromagnetically driven solid density shell implosions in cylindrical and conical geometry [2,3]. These experiments agreed well with two-dimensional magnetohydrodynamic (2D-MHD) calculations—which predicted aluminum liner compressions to 10 Mbar, $3\times$ solid density. We now report on such an experiment in spherical geometry. The experimental results may be useful for comparison with three-dimensional instability theory.

Previous related work by others in cylindrical geometry included that by Alikhanov *et al.* [4], Eskov *et al.* [5], Petrukhin *et al.* [6], Chernyshev *et al.* [7], Turchi *et al.* [8], and Sherwood *et al.* [9]. The deformation of electromagnetically driven cylindrical shells into spheroidal shells has been discussed by Goloviznin *et al.* [10] and by Chernyshev *et al.* [11]. Mokhov discussed 2D-MHD calculations of a spheroidal shell liner driven by an explosive magnetic flux compression generator discharge. Its shape deformed to spherical during the implosion [12]. His publication also showed corroborating radiography from a reduced energy scaled experiment [12]. This achieved a 2 km/sec velocity inferred from comparison of radiography and calculations.

In the work reported here, we used a 12.5 MA, 4.8 MJ capacitor discharge, with current flowing in the polar direction through a spherical aluminum shell between conical electrodes, as illustrated in Fig. 1. This is the first

direct electromagnetically driven spherical liner implosion in the velocity range $\gg 2$ km/sec. Radiography indicates ≥ 7 km/sec of the inner surface at 1 μsec prior to peak compression. 2D-MHD calculations indicate that the liner's peak velocity exceeded 6 km/sec (depth average). The peak inner surface velocity predicted by those calculations is 25 km/sec. The result reported here is also the first example of an electromagnetically imploded liner with an initially spherical shape. The outer surface of the $\pm 45^\circ$ shell is spherical, with 4.0 cm radius. The thickness is proportional to the cosecant squared of the polar angle as measured from the symmetry axis of the electrodes (colatitude). The thickness at the "equator" is 0.10 cm. Deviation of the actual shell thickness from the intended thickness vs polar angle was $\leq 5\%$. The mass was 49 g. The outer surface was polished to a mirror finish. This polar angle variation of thickness causes the ratio of magnetic pressure to shell areal mass density to be independent of polar angle, assuming no polar mass flow. Ideally, this enables the spherical shape to be maintained during the implosion.

To compensate for shell-electrode contact effects, the conical electrodes are overconverged by 3° each. That is, while the zero order design has 45° conical electrodes (whose projected vertices coincide at the origin of the electrode cylindrical coordinate system), the actual design has 42° (with respect to axis) conical electrodes. Their vertices project beyond the midplane from the respective

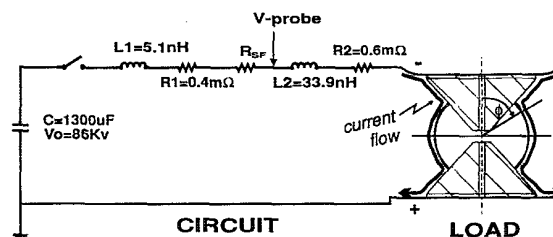


FIG. 1. Circuit diagram and load schematic.

electrodes. These electrodes are truncated at an axial distance of 1 cm from each other (0.5 cm from the origin).

The 1300 μF , 120 kV, 9.4 MJ Shiva Star capacitor bank was used to drive the implosion discharge. The charge voltage and energy were 86 kV and 4.8 MJ. The initial inductance up to the outer surface of the spherical shell was 39 nH. Of this, 33 nH is in a very conservative design vacuum transmission line. This vacuum transmission line inductance can, in principle, be substantially reduced, enabling higher current, faster implosions. The series resistance was approximately 1 m Ω plus the resistance of a safety fuse [2,3]. This 94 cm long, 2.125 cm² cross section aluminum thermister/fuse limits peak discharge current and reversal in the event of an insulator or current feed failure. It has a small but non-negligible effect on a normal discharge. Its resistance during the time of interest ranges from 0.12 to ~ 0.5 m Ω . The peak discharge current, measured by integrated inductive Rogowski and azimuthal magnetic probes, is 12.5 ± 0.5 MA. The current rise time is 9 μsec . The azimuthal magnetic probes indicated full current delivery in the vacuum section of the transmission line for 16 μsec into the discharge. The vacuum chamber pressure was $\sim 10^{-6}$ Torr prior to the discharge.

The principal experimental diagnostic was pulsed radiography, taken with 300 kV, 5 kA, and 30 nsec pulse driven x-ray tubes. The tubes have tungsten anodes (9.13° or 14.25° conical tips), carbon felt cathodes, and 3 mm anode-cathode coaxial gaps. They are normally damaged in such experiments, but readily refurbished. Only cylindrical radial views were used. The source to axis distance is 31.3 cm. The axis to film distance is 37.5 cm. The diagnostic x rays pass through a 0.64 cm thick, 10 cm radius cylindrical outer current conductor and through film pack shielding as well as through the spherical shell. The film pack shielding consists of 0.64 cm aluminum, 3.8 cm polyethylene, and 3.8 cm of low density foam. The film is DuPont NDT 57, with NDT 9 front and back screens. There were three x-ray tubes and film packs used on this experiment. Two were fired at 12.7 μsec and one at 14 μsec into the discharge. Collimation shielding and setup shots eliminated possible crosstalk complications. The earlier radiographs, taken with views 60° apart in azimuth, showed essentially identical images. X-ray pulser timing was confirmed using silicon *p-i-n* x-ray detectors.

Radiographs of the implosion taken at $t = 0, 12.7,$ and 14 μsec into the discharge are shown in Figs. 2 and 3. Also shown are 2D-MHD calculated contours of the inner and outer liner surface. This same calculation was used to generate synthetic radiographs for qualitative comparison with experimental ones. There is good agreement on the experimental and calculated shapes, locations, and timing.

The radiographs show some evidence of short (\sim mm) and long (\sim cm) wavelength nonuniformities. These do not appear to threaten the integrity of the imploding shell. These nonuniformities may be Rayleigh-Taylor instabilities of liquid and plastic portions of the liner.

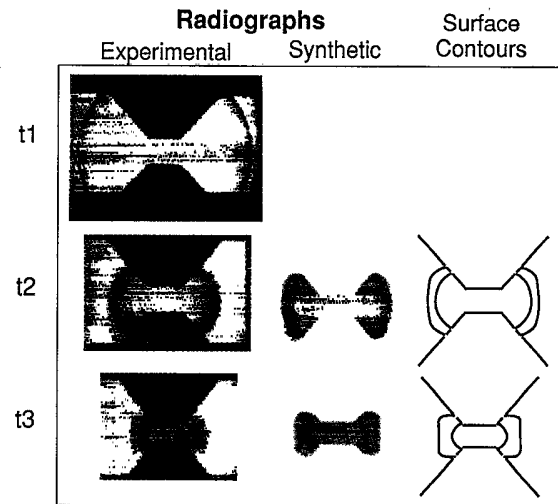


FIG. 2. Radiographs (at $t_1, t_2, t_3 = 0, 12.7, 14 \mu\text{sec}$), 2D-MHD (at $t_2, t_3 = 12.7, 14 \mu\text{sec}$) comparison.

They will be discussed at greater length in a separate paper, for both cylindrical and spherical geometry. The 12.7 μsec radiographs (one shown here) were taken with the sharper 9.13° anode x-ray tubes, which are higher resolution. This may be why the shorter wavelength nonuniformities are more evident than on the 14 μsec radiograph.

The 2D-MHD calculations were done using the CALE code [13,14]. We used version 930313 of this code, with the Steinberg-Guynan elastic-plastic strength model and a 4-phase equation of state for aluminum. We ran this arbitrary Lagrangian-Eulerian (ALE) code in Eulerian mode for ~ 1300 cycles, with 25 axial \times 75 radial zones.

The 2D-MHD calculated synthetic radiographs assume 300 keV monoenergetic x rays and linear film response. The displayed intensities are proportional to chordal path integrals of density times opacity. They may be a more useful comparison to the experimental radiographs than the surface or density contour plots, at least until more complete analysis of the experimental radiographs is accomplished. It should be noted that the experimental radiographs are obtained with a distributed rather than a monoenergetic x-ray spectrum and with nonlinear rather than linear film response. Thus, one expects the synthetic



FIG. 3. Blowup of $t = 14 \mu\text{sec}$ experimental (left) and synthetic (right) radiographs.

radiographs to be an inexact but useful simulation of the experimental radiographs. Good quantitative agreement on shape and symmetry and qualitative agreement on density distribution between synthetic and experimental radiographs are evident.

There is no substantial deviation of the shape of the outer liner surface from spherical either observed or calculated until late in the implosion ($t > 12.7 \mu\text{sec}$, $r < 2.3 \text{ cm}$). The deviation from spherical shape of the outer surface that then occurs is initially consistent with an approximately incompressible liner material. The liner parameters were chosen so that resistive heating would not cause bulk vaporization prior to the liner reaching the axis. Thus, the bulk of the liner material should be solid (albeit plastically deformed) or liquid prior to self-stagnation. If the liner were incompressible and there were no polar mass flow, the outer surface would not implode to a radius less than 1.67 cm at the "equator," nor to a radius less than 2.1 cm at the electrode polar angle. That is, in this approximation, $r_2^3 - r_1^3 = K_0 \csc^2 \phi$, where $K_0 = r_{20}^3 - r_{10}^3$, and r_{20}, r_{10} are the initial outer and inner radii at the equator.

The radius of the liner can be estimated from the circuit inductance. In a low impedance discharge such as this, L_p vs t is obtained from the experimental current I and voltage V_p vs t . V_p is the voltage measured at the (capacitive) voltage probe location, 33.9 nH from the initial liner outer surface position (cf. Fig. 1). We assume that the initial voltage at this position is the inductance ratio (33.9/39) times the charge voltage (86 kV), that is, 75 kV. (L_p is initially 33.9 nH.) The resistance past the voltage probe, R_2 , is approximately 0.6 m Ω and assumed constant. This assumption may be incorrect by $\sim 0.1 \text{ m}\Omega$ over the time of interest. L_p vs t is then obtained in the standard way:

$$L_p = \frac{1}{I} \int_0^t (V_p - IR_2) dt. \quad (1)$$

For self-similar implosion geometry (i.e., electrodes not overconverged), the current radius r_c vs t is related to L_p vs t by

$$\begin{aligned} \Delta L_p &= L_p - L_{p0} \\ &= \frac{1}{I} \int B dA \\ &= 2 \left(\frac{\mu_0}{2\pi} \right) \int_{r_c}^{r_0} \int_{\phi_m}^{\pi/2} \frac{r d\phi dr}{r \sin \phi} \\ &= \frac{\mu_0}{\pi} (r_0 - r_c) \left[-\ln \left(\tan \frac{\phi_m}{2} \right) \right] \\ &= \frac{\mu_0 g}{\pi} (r_0 - r_c), \end{aligned} \quad (2)$$

where ϕ_m is the (colatitude) polar angle of the electrode, r_0 is the initial outer (spherical) current radius (presumably equal to initial outer liner radius), and μ_0 is the magnetic permeability = $4\pi \times 10^{-7} \text{ H/m}$. The geometry factor $g = 0.881$ when $\phi_m = 45^\circ$. The relation is slightly more complicated for overconverged electrodes.

In principle, this analysis gives the current radius vs time. In practice, the errors can be large, with uncertainty in R_2 the major source of error. A reasonable value of R_2 (0.6 m Ω) gives reasonable r_c vs t . Equation (2) is also used to calculate the increasing load inductance (and its derivative dL/dt) in the modeling of the capacitor discharge driving the implosion. In this use, the total series resistance matters, but the calculation is not sensitive to the relative portion of the total resistance past the voltage probe. A comparison of the experimental (spherical) current radius vs time with the 2D-MHD calculated inner and outer liner (spherical) radius r vs time t is shown in Fig. 4. Since the shape deviates from spherical once the incompressible limiting radius at the electrode polar angle is reached, the calculated r vs t is shown for a given polar angle ($\phi = 90^\circ$ equator). This current radius should correspond more to the outer liner radius than to the inner radius, and this is evident in Fig. 4. In the limit of full diffusion of the current throughout the liner thickness, the current radius would correspond to the mean liner radius. 2D-MHD calculations indicate that this current is predominantly limited to the outer 20% of the liner thickness. The more reliable radiography data points are also shown on this plot.

The degree of agreement between experimental and 2D-MHD calculated results encourages us to extend the 2D-MHD predictions through peak compression. Some principal results for a calculation for this experiment are shown in Fig. 5. These indicate that a large portion of the liner mass is compressed to greater than twice solid density, and on the order of 10^{-2} g is compressed to $\sim 6\times$ solid density, 56 Mbar. The predicted inner surface implosion velocity reaches 2.5 to 3 cm/ μsec at a radius of 0.2 cm. The predicted peak implosion kinetic energy is $\sim 1 \text{ MJ}$.

Similar calculations with less conservative electrodes (not overconverged) indicate more distortion of the liner near the electrode, but not enough to cause liner-electrode

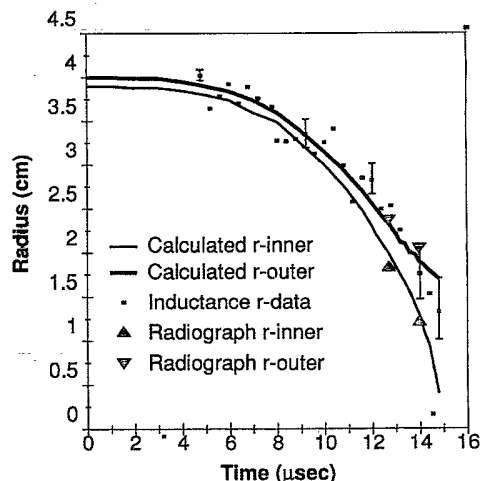


FIG. 4. Calculated, experimental r vs t . Error bars are for $\pm 0.1 \text{ m}\Omega$ tolerance on series resistance R_2 past voltage probe.

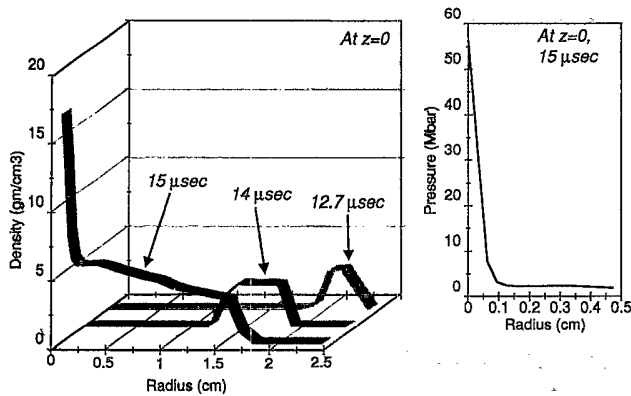


FIG. 5. 2D-MHD calculated density (ρ) vs r at $z = 0$ for 12.7, 14.0, and 15.0 μsec . 2D-MHD calculated pressure (p) vs r at $z = 0$ for peak compression (15.0 μsec).

detachment. Such calculations indicate higher peak compressions, ~ 90 Mbar.

In summary, we have experimentally demonstrated the feasibility of imploding spherical liners with (cylindrically symmetric) magnetic field pressure. This is a basis for creating high energy density matter at high total energy. Experimental results substantially agree with 2D-MHD simulations. Such simulations predict >50 Mbar peak compressions. The degree of agreement with 2D-MHD simulation suggests that three-dimensional instability effects are small.

This research was supported by the Air Force Office of Scientific Research. We would like to acknowledge the support and interest of Dr. W.L. Baker, Dr. B. Godfrey, Dr. R. Kelley, Dr. G. Kiuttu, and Dr. H. Wittmann.

*Present address: US Air Force Academy, Colorado Springs, CO.

†Present address: Physical Sciences, Inc., Alexandria, VA.

‡Present address: Maxwell Laboratories, Inc., Albuquerque, NM.

§Present address: Pennsylvania State University, State

College, PA.

- [1] I. Lindemuth and R. Kirkpatrick, *Nucl. Fusion* **23**, 263 (1983).
- [2] J. Degnan *et al.*, in *Megagauss Technology and Pulsed Power Applications*, Fourth International Conference on Megagauss Magnetic Field Generation and Related Topics, edited by C. Fowler, R. Caird, and D. Erickson (Plenum Press, New York, NY, 1987), pp. 699–706.
- [3] J. Degnan *et al.*, in *Megagauss Fields and Pulsed Power Systems*, Fifth International Conference on Megagauss Magnetic Field Generation and Related Topics, edited by V. Titov and G. Shvetsov (Nova Science Publishers, Inc., New York, NY, 1990), pp. 623–630.
- [4] S. Alikhanov, V. Bakhtin, and D. Toporkov, in *Ultrahigh Magnetic Fields-Physics, Techniques, Applications*, Third International Conference on Megagauss Magnetic Field Generation and Related Topics, edited by V. Titov and G. Shvetsov (Nauka, Moscow, 1984), p. 213.
- [5] A. Eskov, M. Kitayev, and R. Kurtmullayev, in *Ultrahigh Magnetic Fields-Physics, Techniques, Applications* (see Ref. [4]), p. 204.
- [6] A. Petrukhin *et al.*, in *Ultrahigh Magnetic Fields-Physics, Techniques, Applications* (see Ref. [4]), p. 406.
- [7] V. Chernyshev *et al.*, in *Megagauss Technology and Pulsed Power Applications* (see Ref. [2]), pp. 707–712.
- [8] P. Turchi *et al.*, in *Megagauss Physics and Technology*, Second International Conference on Megagauss Magnetic Field Generation and Related Topics, edited by P. Turchi (Plenum Press, New York, NY, 1980), p. 375.
- [9] A. Sherwood *et al.*, in *Megagauss Physics and Technology* (see Ref. [8]), pp. 391–398.
- [10] V. Goloviznin *et al.*, in *Megagauss Physics and Technology* (see Ref. [8]), p. 415.
- [11] V. Chernyshev *et al.*, in "Sixth International Conference on Megagauss Magnetic Field Generation and Related Topics," edited by M. Cowan and R. Spielman (Nova Science Publishers, Inc., Commack, NY, to be published).
- [12] V. Mokhov *et al.*, *Sov. Phys. Dokl.* **24**, 557 (1979).
- [13] R. Tipton, in *Megagauss Technology and Pulsed Power Applications* (see Ref. [2]), p. 299.
- [14] R. Tipton, *CALE Users Manual* (Lawrence Livermore National Laboratory, Livermore, CA, 1990).